Journal of Materials Chemistry A

Accepted Manuscript

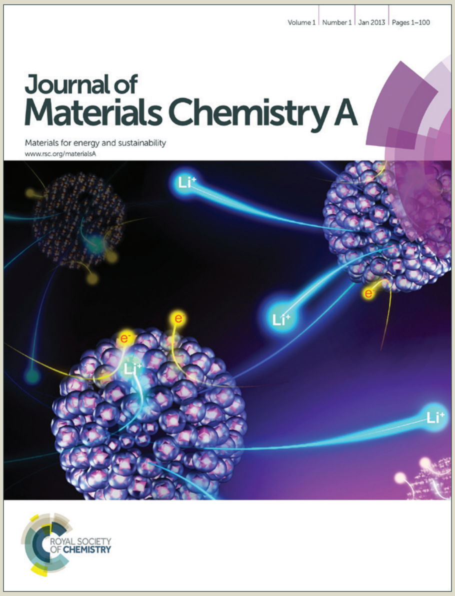

ROYAL SOCIETY OF CHEMISTRY

www.rsc.org/materialsA

Journal of Materials Chemistry A RSCPublishing

ARTICLE

Elaboration of Porous Silicon Carbide by Soft Templating Molecular Precursors with Semi-Fluorinated Alkanes

Cite this: DOI: 10.1039/x0xx00000x

Received 00th January 2012,
Accepted 00th January 2012

DOI: 10.1039/x0xx00000x

www.rsc.org/

T. Nardin,[a] B. Gouze,[a] J. Cambedouzou,*[a] P. Bauduin,[a] M. Wong Chi Man,[b] X. Deschanels,[a] D. Bourgeois,[a] D. Meyer,[a] and O. Diat[a]

We present a novel soft templating approach (STA) for the elaboration of porous silicon carbide (SiC) in oxygen- and moisture-free atmospheres. In this method, the molecular precursor, 1,3,5-trisilacyclohexane (TSCH) which is in a liquid state at room temperature, is templated by a solid network of semi-fluorinated alkanes (SFA) that self-assemble directly in the former liquid. The obtained gel phase is then converted into a polysilane by the polymerization of TSCH molecules around the solid network of SFA. In a next step, the SFA are washed out from the polysilane, and the latter material is converted into SiC by calcination under argon atmosphere at 1000°C. The resulting material possesses a granular structure with a macroporosity. This study validates STA as a sustainable and promising method to obtain porous and mesoporous SiC.

Introduction

Silicon carbides (SiC) are bulk materials which exhibit unique properties such as high temperature stability, oxidation resistance, mechanical resistance or thermal conductivity making them attractive for several fields of application.[1–4] For some fields, such as for nuclear fuel cladding[5] or catalyst supports[6–8] it is desirable to obtain porous SiC in order to provide a better efficiency to the resulting materials. However, it is quite challenging to control the porosity of SiC, namely when it is synthesized at high temperatures. The pyrolysis of polycarbosilanes or polysilanes (as pre-ceramic polymers) consisting of a 1:1 ratio of Si:C content is a remarkable route to SiC but which are obtained as dense materials.[9–11]

One of the main approaches to obtain porous SiC using this route consists in using a sacrificial templating agent[12] which acts as a placeholder during the shaping of the pre-ceramic polymer. Several of these templates are described in the literature ranging from different polymers to sawdust, carbons or silica. The hard templating approach (also known as nanocasting) is, by far, the most common method to obtain porous SiC and can be compared with a moulding process. For example, a porous solid template (eg. SBA-15, KIT-6, CMK-3)[13] is used as a "mould" or rather as a space confiner wherein the precursor is converted into the desired ceramic. This kind of method leads to a ceramic which becomes the inverse replica of the template. However, these solid templates are often difficult to remove from the resulting ceramic, probably due to strong interaction between the solid template and the ceramic SiC (covalent anchoring formed during the process).

Ledoux and coworkers developed an alternative shape-memory synthesis method to prepare porous SiC,[14,15] in which SiC materials are synthesized by the reaction of porous carbon template and gaseous silicon monoxide. In another method, Vix-Guterl *et al.* employed porous SiO_2 templates infiltrated with carbon. The porous SiC materials are produced via the carbothermal reduction of SiO_2.[16,17] An interesting approach was also proposed by Guo *et al.*, consisting in a modified sol-gel route for the preparation of porous SiC.[18,19] The SiC materials are obtained by carbothermal reduction of carbonaceous silicon xerogel.

We propose here an innovative method to develop porous SiC following a "soft templating" approach (STA),[20,21] in a non-aqueous medium without any other solvent than SiC precursors. We introduce here an organosilane as a liquid molecular precursor from which a polycarbosilane can be synthesized by dehydrogenative coupling as a pre-ceramic precursor and which, on pyrolysis, yields the ceramic Si-C. By addition of a soluble directing agent (SDA) which can self-aggregate directly within the liquid organosilane thereby acting as a soft supramolecular template,[22] one can expect to generate porous silicon carbide provided the supramolecular structures are preserved during the subsequent steps: polymerization of the organosilane, the template removal from the resulting polymer and the pyrolysis into ceramic SiC. In this approach, the porosity and the structure of the final materials are therefore defined by the self-assembly of the SDA. The selected molecules are semi-fluorinated

---

[a] ICSM, Institut de Chimie Séparative de Marcoule, UMR 5257, CEA/CNRS/ENSM/Université Montpellier 2, Bat. 426, Site de Marcoule, F-30207 Bagnols-sur-Cèze, France.
[b] ENSCM, Inst Charles Gerhardt Montpellier, UMR CNRS UM2 ENSCM UM1 5253, Lab Architectures Mol & Mat Nanostruct, F-34296 Montpellier, France.
* Corresponding Author. E-mail: Julien.cambedouzou@enscm.fr

† Electronic Supplementary Information (ESI) available: [details of any supplementary information available should be included here]. See DOI: 10.1039/b000000x/

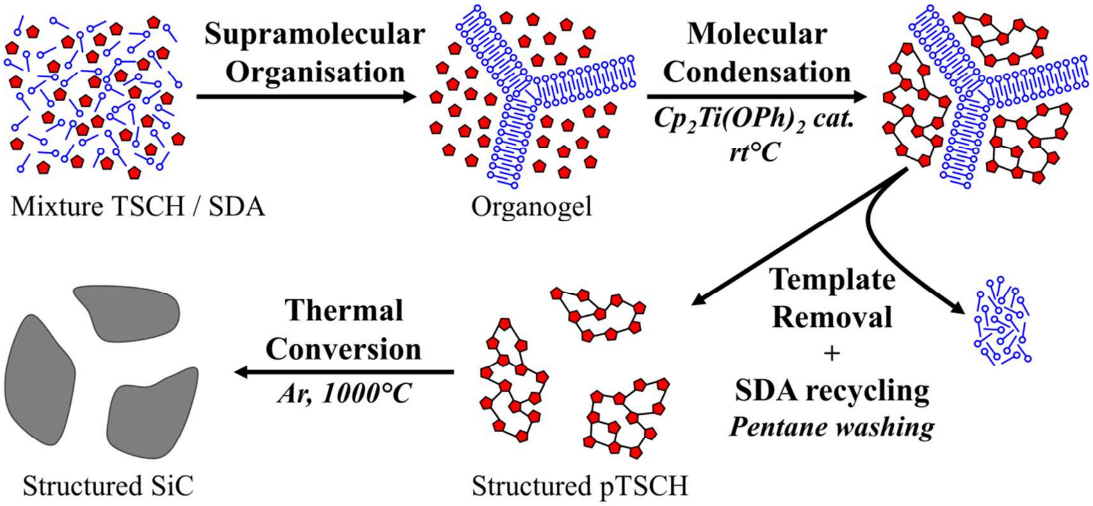

Figure 1 Schematic illustration of the SiC synthesis by STA. The red pentagon represents the molecular SiC precursor and the blue sticks the soluble directing agent (SDA).

alkanes (SFA)[23] as SDA and 1,3,5-trisilacyclohexane (TSCH) as the molecular precursor of the SiC. Interestingly, both molecules are totally anoxic which minimizes the formation of oxy-carbides or silica. SFAs possess an amphiphilic character according to its diblock structure composed of a perfluorinated carbon segment and a hydrocarbon one. TSCH molecules have an affinity with the hydrocarbon segment of SFAs but are not likely to mix with their fluorinated part;[24] this energetic incompatibility is the basic driving force of a self-aggregation in these hydrocarbon media. SFAs are known to form aggregates or gels in oils,[25–29] meaning that they can structure the liquid of precursors which is one of our primary aim in this work. This structured liquid will represent the sought initial state before the polymerization. Then the removal of the SDA compounds and further calcination of the obtained template-free polymer material could result in the formation of a porous SiC. This strategy is summarized in the figure 1.

In this article, we describe first the SiC elaboration starting from TSCH and which is compared to that obtained from a commercial polymeric SiC precursor. Then the self-aggregation behavior of a silylated SFA of chemical formula $C_{12}F_{25}C_2H_4Si(C_2H_5)_3$ (noted $F12SiEt_3$) has been investigated in TSCH. The silyl group of the SFA is expected to favour affinity with the silicon part of the cyclic TSCH. Consequently, the polycarbosilane as well as the final porous SiC material are characterized and compared with corresponding materials elaborated without SDA.

Experimental section

Soluble directing agent (SDA)

$F12SiEt_3$ (see figure 2a), is synthesized by hydrosilylation[30] from triethylsilane and 1H,1H,2H-perfluoro-1-tetradecene in presence of the Karstedt catalyst[31] with a 90% yield (see Supplementary Information). It should be pointed out that $F12SiEt_3$ was used after complete removal of adsorbed moisture by heating at 50°C under vacuum during 2 hours to prevent reaction of the polymeric precursor with any traces of water which will be detrimental to the final SiC (possible formation of silicon oxycarbide).

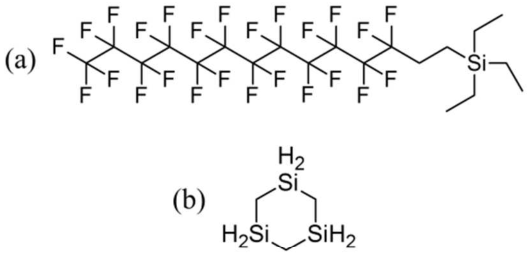

Figure 2 Structural formula of **(a)** the soluble directing agent $F12SiEt_3$ and **(b)** TSCH.

Silicon carbide synthesis

SiC materials were prepared using commercially available TSCH (see figure 2b) or an allyl-hydro-polycarbosilane of commercial denoted SMP10. TSCH of purity higher than 95% was purchased from Gelest and SMP10 from Starfire® Systems. No further purification was applied for these products.

In order to obtain the preceramic polymer, the TSCH is polymerized by catalytic dehydrogenative coupling in a Schlenk flask under argon atmosphere at room temperature using bis(cyclopendienyl)-bis(diphenoxy)titanium ($Cp_2Ti(OPh)_2$) as catalyst[32,33] which was synthesized using an adapted protocol proposed by Andrä[34] (see Supplementary Information).

The dehydrogenative polymerization of TSCH provides the poly-1,3,5-trisilacyclohexane (pTSCH) which is a dense polymeric network[35] (figure 3). Dehydrogenative coupling was also used to promote the cross-linking of SMP10. In this case, the cross-linked polymer will be noted pSMP10.

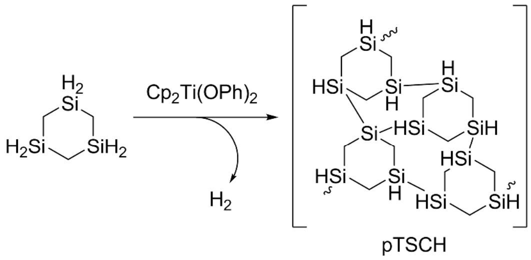

Figure 3 Polymerisation of TSCH by dehydrogenative coupling

A dozen of TSCH/F12SiEt$_3$ mixtures have been prepared for the binary diagram study. Four of them have been study for silicon carbide synthesis, namely those with the following weight fractions: x_w = 0.1, 0.2, 0.35 and 0.5. The F12SiEt$_3$ was added to the TSCH at room temperature under inert atmosphere (Ar). The mixture was stirred and heated at 60°C under argon atmosphere during 10 minutes to solubilize the SDA into the TSCH. Then the mixture was cooled down at room temperature. The four mixtures of TSCH/F12SiEt$_3$ led to the formation of a white organogel below approximately 45°C. The medium was heated again just above the gelation point to return to the liquid state and 1 mol.% of Cp$_2$Ti(OPh)$_2$ was added into the medium. The orange mixture obtained was then heated at 65°C. The activation of the catalyst was highlighted by the medium color change from orange to black after an induction period of approximately 10 minutes. Then the medium is cooled down at room temperature and the polymerization was conducted under static condition at room temperature, i.e. well below the gelation point. The TSCH polymerization during approximately 5 days at room temperature led to a thermosetting plastic material that is insoluble in alkane solvents. Therefore, F12SiEt$_3$ was removed by pentane washing and a porous pTSCH was obtained. The organogelator could be recovered for recycling by distillation.

Pyrolysis of pTSCH or pSMP10 was conducted in alumina crucibles under a flow of argon in a tubular furnace. The heating process was programmed for a 100°Ch^{-1} ramp to 1000 or 1500°C and with a 2 hours plateau at these respective temperatures.

Characterisation

SiC samples were examined by environmental scanning electron microscopy (SEM) using a FEI Quanta 400 FEG. Nitrogen and argon physisorption measurements were performed using a ASAP 2020 at 77K, after outgassing at 623K during 8 hours, reaching a pressure below 1mmHg, and specific surface areas were calculated using the BET method. X-ray diffraction (XRD) measurements were performed using a Bruker diffractometer (Model D8 Advance, Cu Kα radiation; λ = 0.154nm). Small and wide angle X-ray scattering (SWAXS) experiments were conducted on a Xenocs apparatus using a Molybdenum source and delivering a 0.8x0.8mm^2 monochromatic and collimated beam of 0.071nm wavelength. Measurements were carried out in transmission geometry and the scattering patterns were recorded using an online two-dimensional imaging plate detector (MAR-345) located at 750mm from the sample position. The SWAXS experiments were performed as a function of temperature using a sample environment associating a Peltier device and a resistive heater therefore covering a temperature range between -5 and 100°C. A standard procedure for the data treatment was applied, involving an azimuthal averaging and background and empty cell subtraction taking into account the normalization by the acquisition time and the sample transmission. Scattering intensities are given in cm^{-1} after determining an appropriate factor using calibration samples (2.36mm thick high-density polyethylene from Goodfellow®) with well-known scattering values in the small angle range[36]. Thermogravimetric analyses (TGA) were performed in a Setsys 1750 CS Evol under argon at atmospheric pressure and using a heating rate of 5°Cmin^{-1}. Optical microscopy images were recorded using a Zeiss microscope in transmission geometry and between crossed polarizers. Phase transition temperatures between liquids and organogels were estimated by optical microscopy using a Linkam TMS94 temperature controller.

Results and discussion

Generalities

F12SiEt$_3$ exhibits properties of low molecular mass gelators in presence of organic solvents[37] such as alkanes and develops the same behavior with TSCH. Thus TSCH/F12SiEt$_3$ mixtures present properties of thermally-reversible organogel as shown in the next parts.

SMP10 is considered as a good SiC precursor and is used here as a reference. Note that it was not considered for STA since it was not miscible with SDA molecules and that SMP10/F12SiEt$_3$ mixtures did not lead to an organogel.

TSCH polymerization and SMP10 cross-linking are catalyzed by the titanocene Cp$_2$Ti(OPh)$_2$ which is a pre-catalyst. The latter consists of inactive Ti(IV) species which are transformed into active Ti(III) catalyst which conducts the dehydrocoupling catalytic cycle.[38] The conversion of the latent catalyst into the active catalyst occurs at around 65°C in non-oxidative medium. Despite a large amount of studies[39–42] devoted to similar catalysts, the structure of the active catalyst is not completely defined although it is sometimes depicted as a dimetallic complex.[43,44]

Silicon Carbide Synthesis without SDA

TSCH is first polymerized in bulk, leading to the so-called pTSCH. The pyrolysis of this pre-ceramic polymer pTSCH is studied by TGA and the results are compared with that of the polymeric reference pSMP10 (see Supplementary Information, figure S5). The main weight loss is observed in both cases between 350 and 800°C. This temperature range is compatible with the elimination of hydrogen atoms of the polysilanes. In the case of pTSCH, TGA shows a primary weight loss between 150 and 200°C, which corresponds to the elimination of unreacted monomers and dimers of TSCH. A ceramic is obtained at 900°C in both cases, and the total weight loss is 16% and 18% for pSMP10 and pTSCH, respectively.

In a typical conversion procedure, the calcination of the pre-ceramic polymers is performed at 1000 or at 1500°C. According to the XRD and WAXS analysis, the silicon carbides obtained at 1500°C are more crystalline than those obtained at 1000°C (see figure 4.a-b). The diffraction peaks are indeed thinner after a thermal treatment at 1500°C. These peaks are observed at 35.8° (111), 41.8° (200), 60.2° (220) and 71.9° (311) and thus correspond to the crystalline structure of a face-centered cubic β-SiC[45] phase with a lattice constant of 0.434nm (figure 4.a). The peak at 40.2° corresponds to α-Ti which surely originates from catalyst residues. At 1000°C, the diffraction patterns of pTSCH and pSMP10 show β-SiC phase features, albeit widened due to structural disorder. Note that the 220 and 311 peaks are mixed up in a single bump for the pSMP10 at 1000°C, while they are resolved in two bumps for the pTSCH. This difference is an evidence of a less distorted structure in the latter material. The transformation from the amorphous structure towards the crystalline structure is related to the growth of SiC crystalline domains. The size of these domains can be estimated by applying the Scherrer equation to the above-mentioned Bragg peaks.[46,47]

$$\tau_{\text{Scherrer}} = \frac{K\lambda}{\sqrt{(H^2-f^2)}\cos\theta}$$

where K is the shape factor (taken equal to 0.89), λ the X-ray wavelength, H the full width at half maximum (FWHM) of the Bragg peak, f the instrumental resolution (depending on q for the SWAXS diagrams) and θ the Bragg angle.

According to this equation, the crystallite size τ_{Scherrer} grows from 1nm at 1000°C to 4nm at 1500°C for pSMP10, and from 1.5nm at 1000°C to 6nm at 1500°C for pTSCH. The relation between the Bragg angle θ and the scattering vector q is given by the equation

$$q = \frac{4\pi}{\lambda}\sin\theta$$

It is also important to notice that on the XRD patterns as well as on the WAXS diagrams of both samples heated at 1500°C (figure 4.a-b), the (111) peak shows a shoulder at 33.7° ($q = 23.7\text{nm}^{-1}$), attributed to stacking faults[19,48,49]. These stacking faults mainly come from the disordered SiC lattice. During the molecular condensation step, silicon-silicon bonds are formed, but such bonds do not exist in pure SiC. Provided that the temperature conversion is too low to ensure the complete crystallization of the ceramic, the resulting SiC contains some stacking faults.

The SWAXS diagrams of the samples heated at 1000°C display also very broad bumps at scattering vectors $q \sim 1.7\text{nm}^{-1}$ (pTSCH) and 2.5nm^{-1} (pSMP10), which may correspond to distributions of center-to-center mean distances between crystalline domains. This is very similar to what is also observed for semi-crystalline polymers.[50,51] According to this hypothesis, the average distance between crystalline domains would be about 2.5 and 3.7nm for pSMP10 and pTSCH respectively. Residuals of these broad peaks are observed in the 1500°C diagrams at smaller scattering vectors, indicating an increase of the average center-to-center distance between crystallites. This is in line with the growth of crystallite size (figure 4.c).

Finally the X-ray diffraction and SWAXS patterns of the samples treated at 1500°C indicate a slightly distorted β-SiC structure embedded in an amorphous SiC matrix. These observations are in agreement with the literature on polycarbosilane crystallization, according to which a 1500°C pyrolysis does not conduct to fully crystalline ceramics, but rather to a mixture between glassy/amorphous and crystalline SiC.[52–54] β-SiC having a higher density than the amorphous phase, the crystallization occurs at the expense of the latter and cracks appear into the bulk material. Applications requiring a complete transformation of these pre-ceramics into crystalline SiC generally necessitate a higher temperature conversion and densification treatments.[55] In our case, amorphous SiC are acceptable, and thus we will apply a pyrolysis at 1000°C during the elaboration of the porous SiC by STA.

TSCH/F12SiEt$_3$ Gelation Study

Under certain temperature conditions, mixtures of TSCH and F12SiEt$_3$ lead to a thermally-reversible liquid-like/solid-like material

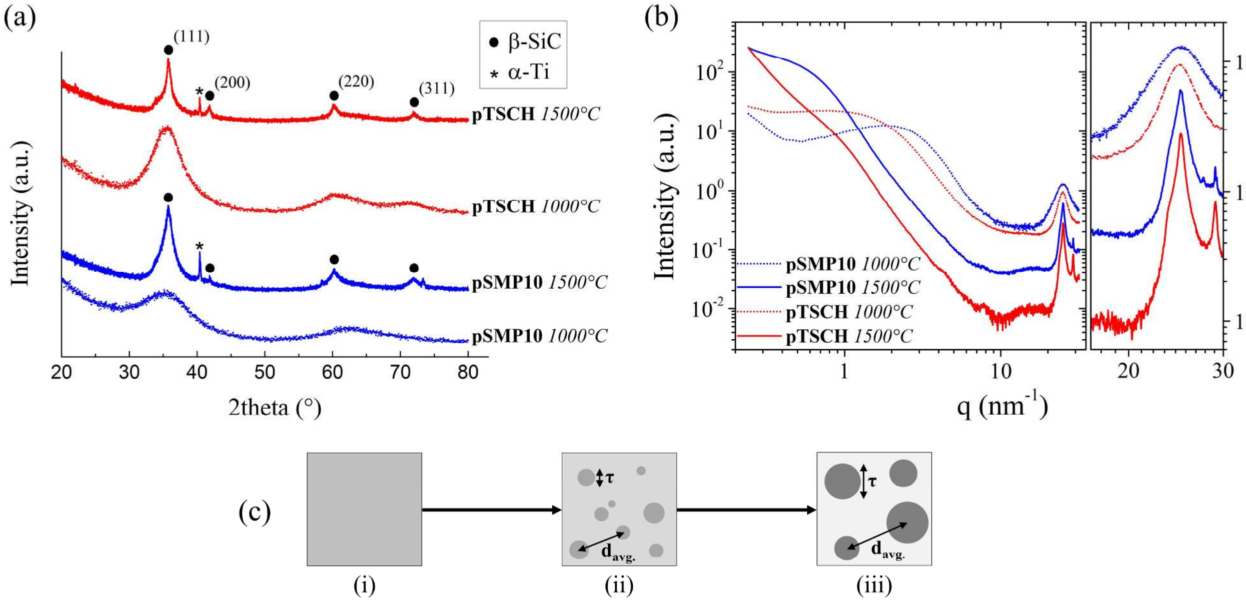

Figure 4 **(a)** Wide-angle XRD patterns and **(b)** SWAXS curves of pTSCH and pSMP10 after heat treatment at 1000 or 1500°C. **(c)** Schematic representation of the crystallization of the amorphous SiC **(i)** into a β-SiC phase obtained at 1000°C **(ii)** or at 1500°C **(iii)** with $d_{\text{avg.}}$ the average center-to-center distance between crystalline domains and τ the crystallite size.

(i.e. *organogel*). We established the binary diagram of the mixture TSCH/F12SiEt$_3$ according to SWAXS results combined with optical microscopy observations (figure 5.a).

Three different phases are revealed in this diagram. Firstly, at high temperature the mixture is monophasic, isotropic and liquid and the blue line represents the transition temperature between this liquid and an organogel. It is interesting to notice that the gelation point is relatively constant (around 45°C) in a range of 0.1 to 0.8 in weight fraction of F12SiEt$_3$. Below this gelation point, the mixture is a white gel. Optical microscopy on organogels evidences a dense network where a solid part stands alongside a liquid part in direct transmission light (figure 5.b-c). In polarized transmission light (figure 5.c), isotropic and birefringent regions as well as smectic-like defects such as Maltese crosses are observed. The smectic-like regions are highlighted by Maltese crosses observed in a thin layer of gel. Finally, the black curve represents another phase transition between two organogels. SWAXS analysis evidences the supramolecular organization of the organogelator in the TSCH solvent. Different SWAXS experiments were carried out varying the weight fraction of F12SiEt$_3$ and the temperature. Characteristic curves of intensities as a function of the scattering vector are given in figure 6 in the case of $x_w = 0.1$. In each of these diagrams the broad peak characteristic of the TSCH solvent liquid order is observed at $q \sim 11.3\text{nm}^{-1}$. The SWAXS experiments at $x_w = 0.2$, 0.35 and 0.5 exhibit similar intensity profiles.

The SWAXS diagrams of the mixtures TSCH/F12SiEt$_3$ (x_w = 0.1, 0.2, 0.35 and 0.5) in the liquid state show an excess of scattering at low q-values that can be analyzed using a form factor of small F12SiEt$_3$ aggregates (aggregation number below 5) in the liquid mixture. Below the gelation point, SWAXS diagrams display Bragg peaks. The organogel n°1 is characterized by the appearance of a lamellar order with a characteristic repeating distance "d_L" at the supramolecular scale and a hexagonal order with a characteristic dimension "d_H" ($d = 2*\pi/q$) at the molecular scale. These characteristic distances do not evolve as a function of solvent content and indicates the presence of crystalline domains within the gel. It certainly corresponds to the skeleton of the organogel[56].

The d_L value taken from SWAXS data is $d_L = 2\pi/2.13 = 2.95$nm. According to the equation

$$le = (1.67 + 0.1265n + 0.15)\text{nm}$$

proposed by P. Marczuk and P. Lang[57] where *le* is the length of a $F(CF_2)_{12}(CH_2)_nH$ molecule with a 12-carbon atom fluorinated alkyl chain, the length of a F12SiEt$_3$ molecule is approximately equal to 2.45nm. Thus, d_L could correspond to the length of two F12SiEt$_3$ molecules in a head to tail configuration (see figure 6 b.i). It evolves from 2.95nm to 2.81nm when decreasing the temperature in the zone B. This decrease reveals a contraction of the lamellae by cooling. The phase transition T_{gel} n°2 is characterized by a sudden decreasing of "d_L" from 2.81 to 2.69nm (see Supplementary Information). "d_H" corresponds to the 10 distance in the 2D hexagonal stacking of the F12SiEt$_3$ inside lamellae (see figure 6.b.iii) and does not noticeably evolve with temperature. The lattice parameter "a_H" of this hexagonal packing can be deduced from the relation: $d_H = a_H * \cos(\pi/6)$. "a_H" is approximately 0.6nm, which is nearly the diameter of a stick (0.59nm).[25] This information gives a detailed overview of the supramolecular organization of F12SiEt$_3$ molecules at the nanoscopic scale (figure 6.b). Thus, in good agreement with optical microscopy, SWAXS diagrams highlight the presence of smectic-like phases corresponding to a lamellar organization of the F12SiEt$_3$ molecules. The organogel can be seen as a biphasic structure where one liquid domain (TSCH) is embedded within a solid and organic network. It is proposed that the sudden phase transition T_{gel} n°2 (figure 5.a, black curve) corresponds to a transition between a smectic A symmetry and a smectic C symmetry into this solid phase. In the smectic A phase, the molecules of F12SiEt$_3$ are oriented along the lamellae and perpendicular to the lamellar plane, while they are tilted away from the lamellar plane in the smectic C phase. This phase transition occurs at around T = 5°C in the [0.1; 0.8] range of weight fraction of F12SiEt$_3$. Keeping in mind that we intend to transform the gel into a polysilane by a catalytic reaction, only the smectic A phase will be considered as interesting since the domain of existence of the smectic C phase corresponds to temperatures which are too low to achieve the polymerization in a reasonable time.

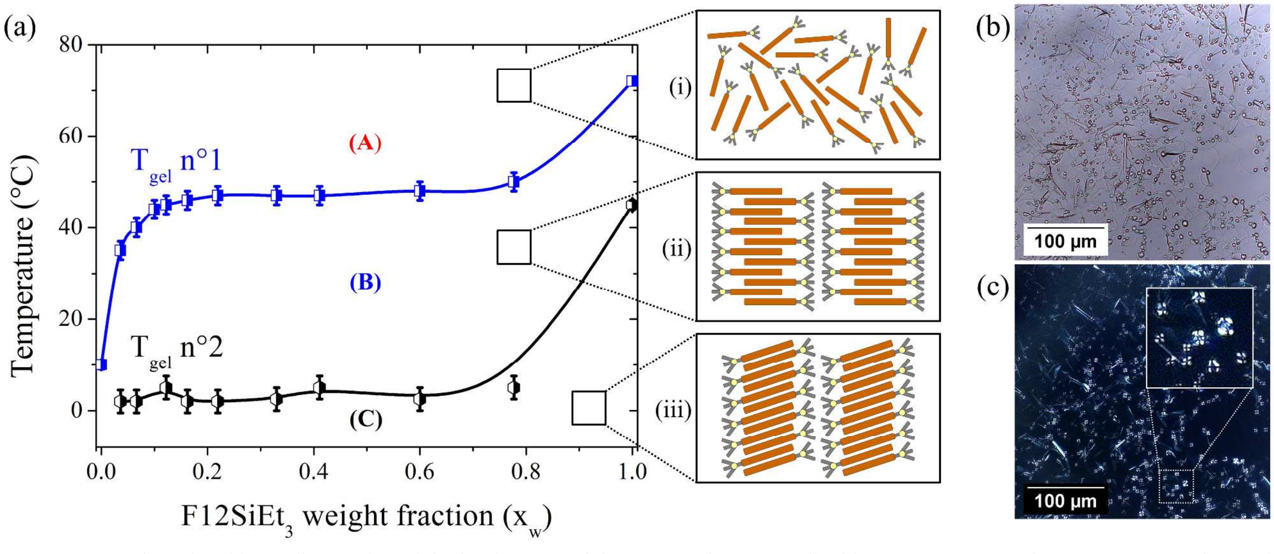

Figure 5 (a) TSCH/F12SiEt$_3$ binary diagram in weight fraction (x_w) of the organogelator – (A) liquid state; (B) organogel n°1; (C) organogel n°2 with schematic representation of molecular packing proposed for F12SiEt$_3$ into TSCH in the regions A **(i)**,B **(ii)** and C **(iii)**. The orange elongated rectangles represent the fluorinated alkyl group of F12SiEt3 and the grey ones the alkyl group. Silicon appears in yellow. Optical microscopy images on a binary mixture TSCH/F12SiEt$_3$ (x_w = 0.1) at room temperature in direct transmission light **(b)** and in polarized transmission light **(c)**.

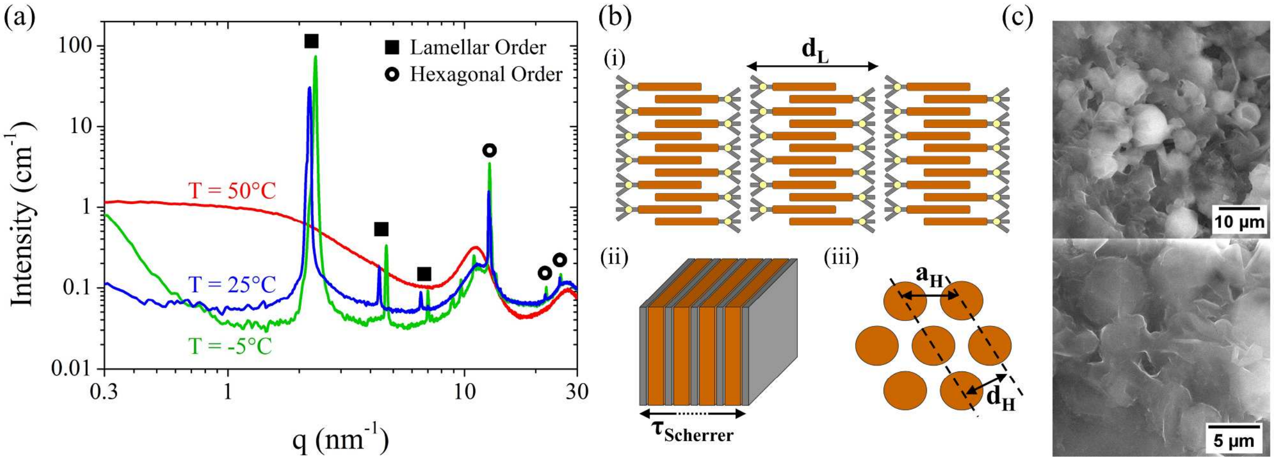

Figure 6 **(a)** SWAXS diagrams on a binary mixture TSCH/F12SiEt$_3$ (x_w = 0.1) in the liquid state (*T = 50°C, red curve*), on the organogel n°1 (*T = 25°C, blue curve*) and on the organogel n°2 (*T = -5°C, green curve*). **(b)** Schematic representations of the molecular packing proposed for F12SiEt$_3$ in TSCH. The orange elongated rectangles represent the fluorinated alkyl group of F12SiEt$_3$ and the grey ones the alkyl group. Silicon appears in yellow. **(i)** Proposed molecular organization in lamellae, **(ii)** in crystallites formed by lamellae and **(iii)** side view of the hexagonal organization of the fluorinated part of F12SiEt$_3$ molecules in a lamella. a_H corresponds to the lattice parameter of the hexagonal lattice, and d_H corresponds to the 10 reticular distance. **(c)** SEM images of the solid network looking as connected flakes of organogelators into a mixture TSCH/F12SiEt$_3$ (x_w = 0.1) at low temperature.

Furthermore, the Scherrer equation gives a characteristic size of the crystallites τ_{Scherrer} in the organogel n°1 of 160 ± 40 nm (figure 6.b.ii) independently of the F12SiEt$_3$ weight fraction. The invariance of the gelation temperature as well as that of the crystallite size versus the organogelator weight fraction reveals that the organogelator concentration only impacts on the solid network density in the TSCH solvent. SEM images shown in figure 6.c present the morphology of this solid network. In these images, the TSCH was degassed and consequently only the solid skeleton of the gel remains. This solid network divides the solvent phase in domains and therefore can be used as a templating agent for the solvent polymerization.

Silicon Carbide Synthesis by STA

After having described the TSCH/F12SiEt$_3$ mixture, we focused on the polymerisation of TSCH with different SDA concentrations. Four different weight ratios of TSCH/F12SiEt$_3$ (x_w = 0.1, 0.2, 0.35 and 0.5) were chosen for which 1%mol of catalyst was used in each of these samples. Typically, after heating the medium at 65°C to induce the catalytic activity, the polymerization was then conducted at room temperature. Due to the slow kinetic of the dehydrogenative coupling at room temperature, the reaction lasted for about 6 days. It is important to notice that the polymerization did not occur in the case of x_w = 0.5 probably due to the low diffusion factor of the catalyst into the medium. Once the polymerization of TSCH was achieved, the resulting mixture was washed with pentane in order to remove and recycle the F12SiEt$_3$ and a structured pTSCH was obtained.

The three successfully obtained polymeric pTSCH materials exhibit granular morphologies with stacked grains of mean diameter ≈ 100, 240 and 270 nm respectively from mixtures x_w = 0.1, 0.2 and 0.35, and is exemplified in figure 7.c by the polymer obtained in the case of x_w = 0.1. The morphology of these materials appears strikingly different from that of the reference pTSCH (figure 7.a), revealing the role of the structuring agent played by the F12SiEt$_3$.

We propose here that the observed grains result from the TSCH segregation in regions separated by the SDA solid network. The latter solid network therefore acts as a continuous “mould” during the polymerization of TSCH precursors, and it is integrally removed by pentane during the washing step. The volume formerly occupied by F12SiEt$_3$ results in the porosity of the material. Note that the dehydrogenative coupling between TSCH molecules induces a hydrogen release which could destabilize the organogel organization. For this reason, the obtained pTSCH is not necessarily the exact replica of the solid network of the SDA in the initial gel. Nevertheless, the order of magnitude of the typical distances in the pTSCH is approximately equivalent to that in the organogel.

The final SiC materials are obtained after pyrolysis of the pTSCH at 1000°C. EDX analyses gave a Si:C ratio close to 1:1 and an oxygen content lower than 5 at.%. This tends to indicate that there is almost no SiO$_2$ nor pure carbon in the final materials. A SEM image of the SiC derived from the mixture at x_w = 0.1 is displayed in figure 7.d (for x_w = 0.2 and 0.35 see in Supplementary Information, fig S7). It shows that the granular morphology of the pTSCH is preserved in the SiC ceramic. The grain size appears slightly reduced which probably originates from the densification of the material during the thermal treatment. The small and wide angle X-ray scattering pattern of the porous SiC material displays the same profile as the one obtained for the reference SiC originating from pure TSCH without SDA. This result shows that the structure of the porous SiC is identical to that of the reference non porous SiC for typical distances lower than 30nm. It is in line with the observations made on SEM images, showing grains of typical size of about 100 to 300nm. Moreover, no mesoporosity and no microporosity likely exist in porous SiC. Gas adsorption experiments were performed on the soft-templated SiC and tend to confirm the absence of meso- and micro-pores. A specific surface of 30.2m^{2}g^{-1} is indeed measured on the porous SiC derived from the mixture at x_w = 0.1. Considering that a maximum value of 60m^{2}g^{-1} would be expected for spheres of diameter 100 nm, for which the total surface would be accessible, the specific surface obtained here is in good agreement with the hypothesis of partially connected non porous grains of SiC (see in Supplementary Information, fig S8 and related text). Therefore, the porosity of this SiC material can be viewed as the voids between dense grains, forming a continuous multi-connected space of typical lateral dimension of about 100 nm, i.e. the typical size of dense grains.

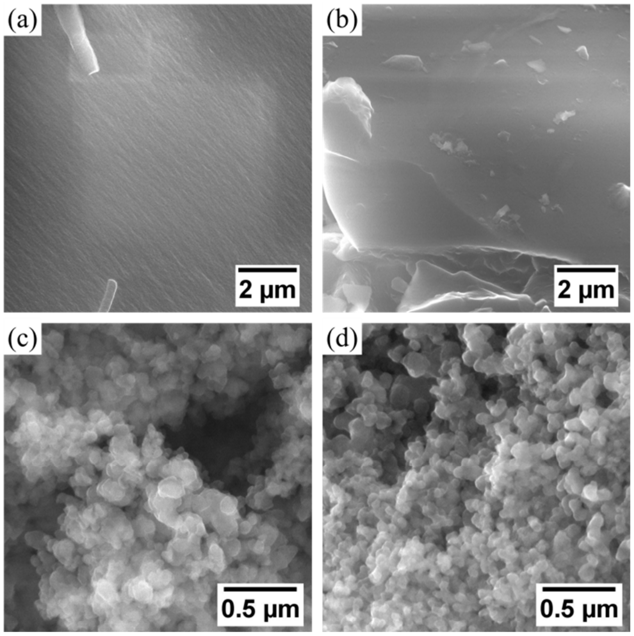

Figure 7 SEM images of **(a)** pTSCH, **(b)** SiC from pTSCH at 1000°C, **(c)** porous pTSCH obtained by 25°C molecular condensation of TSCH into a $x_w = 0.1$ $F12SiEt_3$ organogel and **(d)** porous SiC resulting from the pyrolysis at 1000°C of pTSCH obtained by 25°C molecular condensation of TSCH into a $x_w = 0.1$ $F12SiEt_3$ organogel.

Table 1 summarizes the surface areas measured on the different SiC samples obtained from media containing different TSCH/SDA weight ratios. It shows that the specific surface areas of all materials range from 18 to $31 m^2g^{-1}$, in good agreement with the macroporous grain-like structure described above. The reason for the increase of the grain diameter and the decrease of the specific surface area when increasing the SDA weight fraction is unclear. We could however formulate an hypothesis according to which the increase of the SDA weight fraction would result in the enlargement of the walls of the solid network together with the volume of the segregated regions of TSCH. Such a change in the gel structure would result in the increase of the grain size and the decrease of the specific surface area, as observed experimentally.

Conclusions

The polymerization and transformation of a new type of molecular SiC precursor TSCH into silicon carbide at 1000°C have been studied and compared primarily with those obtained from a commonly used polymer, SMP10. The synthesis steps from the monomer *via* the corresponding cyclic polysilane (pTSCH) to the final SiC ceramic were optimized and fully characterized. The preceramic pTSCH polymer obtained from TSCH possesses similar properties to the commercial polymer SMP10 regarding the pyrolysis process. However, TSCH has the major advantage of offering the possibility to act as a good organic solvent allowing the formation of an organogel with low molecular mass gelators such as $F12SiEt_3$. A detailed investigation was then performed on the binary mixture TSCH/$F12SiEt_3$ which allowed a precise description of the supramolecular structures of the resulting organogel. This organogel is constituted of a solid network of the organogelator $F12SiEt_3$ which creates segregated regions of liquid TSCH in the mixture. The solid network was characterized as lamellae of $F12SiEt_3$.

The polymerization of TSCH was conducted with $Cp_2Ti(OPh)_2$ as dehydrogenative catalyst on mixtures with TSCH/$F12SiEt_3$ weight ratios of 0.1, 0.2, 0.35 and 0.5, the first three leading to structured pTSCHs while the last one failed due to the lack of catalytic reaction in this case. The pyrolysis of these three pTSCHs under argon atmosphere yielded porous SiC. Compared with a typical SiC synthesized from TSCH without SDA (which resulted in a bulk and dense morphology with a surface area $< 1 m^2g^{-1}$), here the SDA-made SiC consisted of agglomerated nanograins (diameter size ranging from 100 to 300nm) exhibiting appreciable specific surface areas (18 to $30 m^2g^{-1}$) attributed to interconnecting voids created by the removal of agregates of the gelator after the polymerization of the TSCH into pTSCH and which could be preserved while transforming the latter into SiC at 1000°C.

In summary, we elaborated porous SiC using an original soft templating approach. Contrarily to the commonly used hard templates (silica…) prone to formation of oxycarbides, in this approach, the medium is oxygen-free, and the probability of forming oxycarbides is therefore minimized. It is important to notice here that STA allows a recycling of the SDA and, moreover it can be viewed as a solvent-free approach, as the TSCH plays both the role of reagent and solvent. With these advantages, the STA can be considered as a process that is consistent with the goals of sustainable chemistry. Although the initial aim of obtaining mesoporous SiC was not completely achieved, the results of these studies confirm the feasibility of our STA approach and can be validated as a promising method to obtain porous and mesoporous SiC. Considering new SDA should allow obtaining mesoporous materials of higher specific surface. The requirements for this approach would be to have (1) a low mass gelator able to form an organogel with TSCH (or any other organosilane with Si/C ratio close to 1 susceptible to polycondense by dehydrogenative coupling), (2) preservation of the resulting organogel at high temperature allowing a fast polymerization step and (3) the presence of mesostructuration thanks to the soft templating agent in the solid network to ensure a high specific surface of the resulting SiC.

Acknowledgements

The authors would like to thank the French CNRS NEEDS-Matériaux (2012-2013) and the French ANR program (Fanta_SiC project, ANR-12-JS08-0010-01) for the financial support on this work. The authors acknowledge C. Rey for assistance on gas adsorption operation, B. Corso for help on X-ray scattering, and J. Ravaux for SEM operation. X. Cattoën is thanked for scientific contributions.

x_w ($F12SiEt_3$)	Gelation Point (± 2°C)	Final SiC Grain Mean Diameter (nm)	Final SiC Specific Surface Area (m^2g^{-1})
0	n.a.	n.a.	< 1
0.1	44	100	30.2
0.2	47	240	20.1
0.35	47	270	18.5
0.5	47.5	n.a.	n.a.

Table 1 Final SiC characteristics. Grain mean diameter is determined by SEM images treatment using an open source image processing package based on the ImageJ software.[58]

Notes and references

1 J. B. Casady and R. W. Johnson, *Solid-State Electron.*, 1996, **39**, 1409–1422.
2 M. Singh, *J. Mater. Sci. Lett.*, 1998, **17**, 459–461.
3 M. Willander, M. Friesel, Q. U. Wahab and B. Straumal, *J. Mater. Sci.-Mater. Electron.*, 2006, **17**, 1–25.
4 K. M. Pitman, A. M. Hofmeister, A. B. Corman and A. K. Speck, *Astron. Astrophys.*, 2008, **483**, 661–672.
5 S. Bragg-Sitton, K. Barrett, I. van Rooyen, D. Hurley and M. Khafizov, *Nucl. Eng. Int.*, 2013, **58**, 37–40.
6 M. J. Ledoux and C. Pham-Huu, *Cattech*, 2001, **5**, 226–246.
7 R. Moene, M. Makkee and J. A. Moulijn, *Appl. Catal. -Gen.*, 1998, **167**, 321–330.
8 M. Vannice, Y. Chao and R. Friedman, *Appl. Catal.*, 1986, **20**, 91–107.
9 R. Corriu, M. Enders, S. Huille and J. Moreau, *Chem. Mater.*, 1994, **6**, 15–17.
10 R. West, L. David, P. Djurovich, H. Yu and R. Sinclair, *Am. Ceram. Soc. Bull.*, 1983, **62**, 899–903.
11 S. Yajima, Y. Hasegawa, J. Hayashi and M. Iimura, *J. Mater. Sci.*, 1978, **13**, 2569–2576.
12 L. Borchardt, C. Hoffmann, M. Oschatz, L. Mammitzsch, U. Petasch, M. Herrmann and S. Kaskel, *Chem. Soc. Rev.*, 2012, **41**, 5053–5067.
13 H. Tüysüz, C. W. Lehmann, H. Bongard, B. Tesche, R. Schmidt and F. Schüth, *J. Am. Chem. Soc.*, 2008, **130**, 11510–11517.
14 N. Keller, C. Pham-Huu, M. J. Ledoux, C. Estournes and G. Ehret, *Appl. Catal. Gen.*, 1999, **187**, 255–268.
15 J.-M. Nhut, R. Vieira, L. Pesant, J.-P. Tessonnier, N. Keller, G. Ehret, C. Pham-Huu and M. J. Ledoux, *Catal. Today*, 2002, **76**, 11–32.
16 J. Parmentier, J. Patarin, J. Dentzer and C. Vix-Guterl, *Ceram. Int.*, 2002, **28**, 1–7.
17 C. Vix-Guterl, I. Alix and P. Ehrburger, *Acta Mater.*, 2004, **52**, 1639–1651.
18 G.-Q. Jin and X.-Y. Guo, *Microporous Mesoporous Mater.*, 2003, **60**, 207–212.
19 Y.-J. Hao, G.-Q. Jin, X.-D. Han and X.-Y. Guo, *Mater. Lett.*, 2006, **60**, 1334–1337.
20 Y. Wan, Y. Shi and D. Zhao, *Chem. Commun.*, 2007, 897–926.
21 L. Borchardt, M. Oschatz, M. Lohe, V. Presser, Y. Gogotsi and S. Kaskel, *Carbon*, 2012, **50**, 3987–3994.
22 R. Laversanne, *Macromolecules*, 1992, **25**, 489–491.
23 J. F. Rabolt, T. P. Russell and R. J. Twieg, *Macromolecules*, 1984, **17**, 2786–2794.
24 B. P. Binks, P. D. I. Fletcher, S. N. Kotsev and R. L. Thompson, *Langmuir*, 1997, **13**, 6669–6682.
25 M. P. Krafft and J. G. Riess, *Chem. Rev.*, 2009, **109**, 1714–1792.
26 M. Broniatowski and P. Dynarowicz-Łątka, *Adv. Colloid Interface Sci.*, 2008, **138**, 63–83.
27 P. L. Nostro, *Curr. Opin. Colloid Amp Interface Sci.*, 2003, **8**, 223–226.
28 T. P. Russell, J. F. Rabolt, R. J. Twieg, R. L. Siemens and B. L. Farmer, *Macromolecules*, 1986, **19**, 1135–1143.
29 R. J. Twieg, T. P. Russell, R. Siemens and J. F. Rabolt, *Macromolecules*, 1985, **18**, 1361–1362.
30 A. M. LaPointe, F. C. Rix and M. Brookhart, *J. Am. Chem. Soc.*, 1997, **119**, 906–917.
31 L. N. Lewis, *Platin. Met. Rev.*, 1997, **41**, 66–75.
32 S. Bourg, R. J. P. Corriu, M. Enders and J. J. E. Moreau, *Organometallics*, 1995, **14**, 564–566.
33 J. Garcia, D. J. M. Meyer, D. Guillaneux, J. J. E. Moreau and M. Wong Chi Man, *J. Organomet. Chem.*, 2009, **694**, 2427–2433.
34 K. Andrä, *J. Organomet. Chem.*, 1968, **11**, 567–570.
35 J. Garcia, PhD Thesis, Université Montpellier 2, 2008.
36 J. Cambedouzou and O. Diat, *J. Appl. Crystallogr.*, 2012, **45**, 662–673.
37 P. Terech and R. G. Weiss, *Chem. Rev.*, 1997, **97**, 3133–3160.
38 J. F. Harrod, *Coord. Chem. Rev.*, 2000, **206–207**, 493–531.
39 B. A. Goldslager and S. J. Clarson, *J. Inorg. Organomet. Polym.*, 1999, **9**, 123–131.
40 A. D. Sadow and T. D. Tilley, *Organometallics*, 2003, **22**, 3577–3585.
41 T. D. Tilley, *Acc. Chem. Res.*, 1993, **26**, 22–29.
42 J. Y. Corey, *Chem. Rev.*, 2011, **111**, 863–1071.
43 C. T. Aitken, J. F. Harrod and E. Samuel, *J. Am. Chem. Soc.*, 1986, **108**, 4059–4066.
44 E. Samuel and J. Harrod, *J. Am. Chem. Soc.*, 1984, **106**, 1859–1860.
45 E. Whitney, *Nature*, 1963, **199**, 278–280.
46 U. Holzwarth and N. Gibson, *Nat. Nanotechnol.*, 2011, **6**, 534–534.
47 W. Gruber, H. H. Najafabadi, U. Geckle, M. Bruns and H. Schmidt, *Philos. Mag.*, 2010, **90**, 3855–3865.
48 Y. Sugahara, Y. Takeda, K. Kuroda and C. Kato, *J. Mater. Sci. Lett.*, 1989, **8**, 944–946.
49 S. Pan, Y. Yang, J. Zhang and G. Song, *J. Mater. Sci.*, 2005, **40**, 4679–4681.
50 A. Saffar, A. Ajji, P. J. Carreau and M. R. Kamal, *Polymer*, 2014, **55**, 3156–3167.
51 N. Stribeck, A. A. Camarillo, U. Nöchel, P. Bösecke and R. K. Bayer, *Anal. Bioanal. Chem.*, 2007, **387**, 649–661.
52 D. Kurtenbach, H.-P. Martin, E. Müller, G. Roewer and A. Hoell, *J. Eur. Ceram. Soc.*, 1998, **18**, 1885–1891.
53 M. Yan, W. Song and C. Zhao-hui, *Ceram. Int.*, 2010, **36**, 2455–2459.
54 P. Colombo, T. E. Paulson and C. G. Pantano, *J. Am. Ceram. Soc.*, 1997, **80**, 2333–2340.
55 Z. Luo, X. Zhou, J. Yu, K. Sun and F. Wang, *Ceram. Int.*, 2014, **40**, 1939–1944.
56 C. Y. Ku, P. LoNostro and S. H. Chen, *J. Phys. Chem. B*, 1997, **101**, 908–914.
57 P. Marczuk and P. Lang, *Macromolecules*, 1998, **31**, 9013–9018.
58 J. Schindelin, I. Arganda-Carreras, E. Frise, V. Kaynig, M. Longair, T. Pietzsch, S. Preibisch, C. Rueden, S. Saalfeld, B. Schmid, J.-Y. Tinevez, D. J. White, V. Hartenstein, K. Eliceiri, P. Tomancak and A. Cardona, *Nat. Methods*, 2012, **9**, 676–682.

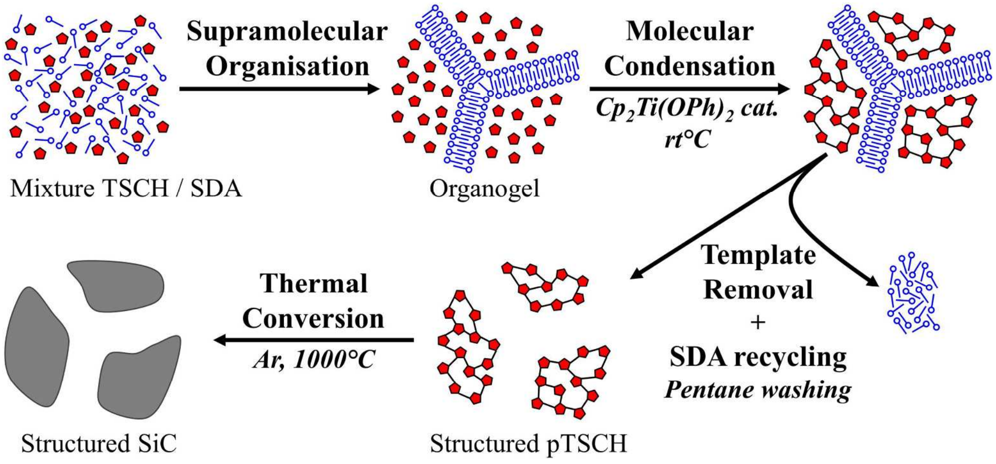

446x210mm (150 x 150 DPI)